Silicon Oxide Cluster Formation and Stability in the Laser Ablation of SiO Targets

María Jadraque,*,† Magna Santos,‡ Luís Díaz,‡ Jesús Álvarez-Ruiz,† and Margarita Martín†

Instituto de Química Física "Rocasolano", CSIC, Serrano 119, 28006 Madrid, Spain, and Instituto de Estructura de la Materia, CSIC, Serrano 123, 28006 Madrid, Spain

Received: January 28, 2009; Revised Manuscript Received: August 25, 2009

The formation mechanism and stability of silicon oxide clusters observed in the ablation of SiO targets at 266 nm were investigated by time-of-flight mass spectrometry, laser-induced fluorescence (LIF), and DFT calculations. Neutral and positively charged $Si_n^{+/0}$ and $Si_nO_mH_{0,1}^+$ clusters were identified in the plume, but neutral Si_nO_m could not be observed. The time distribution of SiO in the plume measured by postionization with an ArF laser ($\Delta\lambda \approx 1$ nm, $\tau \approx 14$ ns) and mass spectrometric detection was compared with that obtained by LIF with narrowband dye laser selective excitation of one specific rovibronic transition in SiO. Postionization leads to a multicomponent distribution that extends up to times near 100 μs after ablation, whereas LIF measurements obtain time distributions shorter than 20 μs. DFT calculations of several $Si_nO_m^{0/+}$ were performed, showing that one photon absorption of the postionization laser makes available low-energy dissociation channels of the neutrals, whereas two photon absorption is required for ionization. DFT calculations were carried out for stoichiometric H-containing clusters $Si_nO_nH^+$ ($n = 1-4$). For $n = 1,2$, the optimized geometries involve bonding of hydrogen to one oxygen atom in the clusters; for $n = 3$ and 4, the structures containing H–Si bonds are more stable.

1. Introduction

Interest in silicon oxide clusters is increasing after the discovery of their fundamental role in the growth and final properties of nanosized materials. Experimental and theoretical work have reported that silicon suboxide clusters, especially silicon monoxide, are involved in the growth of silicon nanowires.[1–5]

The optical properties of silicon oxide clusters are dependent not only on size but also on the degree of oxidation. Theoretical calculations predict that small Si_nO_m clusters (n, $m \leq 8$) may have a strong influence on the optical properties of materials with embedded silicon nanoparticles because of the remarkable energy gap dependence on oxygen content.[6] This is consistent with the significantly different properties found for the above materials under different synthesis conditions; for instance, the photoluminescence spectrum of cluster deposits formed by laser ablation of silicon targets significantly changes when ablation takes place in the presence of small amounts of oxygen.[7]

Hydrogen defects also influence the properties of silicon oxide nanostructures; for instance, the performance of devices based on silicon-rich oxide (SRO) nanodeposits is strongly dependent on their hydrogen content.[8] The hydrogen atom can bond in different configurations, and the dominant defect type depends on the stoichiometry of the material.

Free silicon oxide clusters of different stoichiometry can be generated by evaporation and laser ablation or sputtering of sources containing SiO, SiO_2, or Si and O_2.[9,10] In the ablation of SiO at the laser wavelengths of 308 nm, we have reported the formation of silicon oxide cationic clusters and neutral and cationic Si_n clusters;[11,12] however, no neutral Si_nO_m were detected, although DFT calculations predict stable configurations for the above clusters under normal conditions;[13–15] moreover,

relatively large fragmentation energies have been calculated for several Si_7O_n neutral clusters.[16] At the ablation wavelengths of 10.53 μm and 308 nm, it has also been reported that the target decomposes by thermal ablation via disproportionation of SiO, resulting in the development of Si islands in the ablated spots.[17]

In this work, we have investigated the formation of silicon oxide clusters using ablation of SiO at the laser wavelength of 266 nm, where the mechanism is nonthermal and disproportionation of the target has not been observed, at least in the range of fluences spanned in this work.[18] Time-of-flight mass spectrometry, computational methods, and laser-induced fluorescence (LIF) are used to investigate the formation mechanisms and stability of cationic and neutral silicon oxide clusters. The results can provide guidelines toward the design of strategies for the controlled synthesis of silicon oxide nanostructures. Also, in this work, we have investigated the structure of H-containing clusters; it has been pointed out that atoms in small clusters can all be considered to be surface atoms; therefore, understanding the bond structure of those small clusters can help us to get insight into the H-bonding of siliceous surfaces and nanodeposits.[19]

2. Experimental and Computational Methodology

Pressed pellets of SiO were ablated under vacuum conditions better than 2×10^{-6} mbar by the focused output of the fourth harmonic of a Nd/YAG (266 nm) laser. Cluster composition of the ablation plume was investigated by TOF-MS (time-of-flight mass spectrometry). The target was placed between the repelling and extracting plates of a linear TOF-MS, with target surface parallel to the flight axis of the mass spectrometer and at variable distances from the flight axis; an electric field typically in the range of 45–250 V·cm^{-1} deflected the ions along the TOF axis. Neutral species in the plume were observed by ArF laser (193 nm, $\Delta\lambda \approx 1$ nm) postionization. Laser energies were limited by variable apertures to values in the range of 0.1 to 2.5 mJ. The laser beam mildly focused by a 40 cm focal length lens

* Corresponding author. E-mail: Jadraque@iesl.foth.gr. Tel: +34 561 94 00.
† Instituto de Química Física "Rocasolano", CSIC.
‡ Instituto de Estructura de la Materia, CSIC.

Silicon Oxide Cluster Formation and Stability

J. Phys. Chem. A, Vol. 113, No. 41, 2009 **10881**
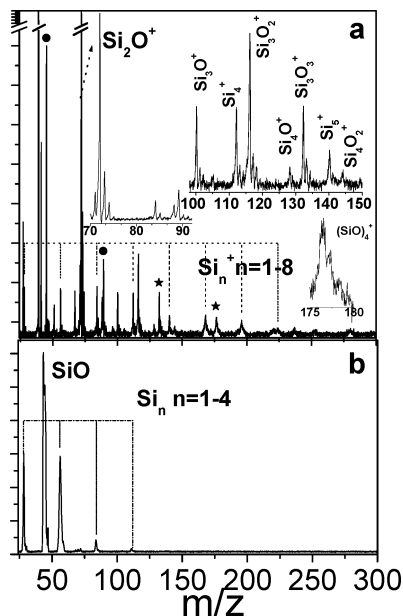
Figure 1. Ablation of SiO targets at 266 nm. (a) Mass spectra of positive ions in the plume obtained at a laser fluence of 0.2 J·cm^{-2}. Peaks marked with an asterisk are $(SiO)_n^+$ ($n = 3, 4$). Peaks marked with full circles are $m/z = 45$ and 89 assigned to $SiOH^+$ and $Si_2O_2H^+$, respectively. The insets show expanded views of the m/z regions 70−90 amu, 100−150, and 175−180 amu. Unlabeled peaks are impurities. (See the text.) (b) Mass spectra of neutral species in the plume observed by postionization with an ArF laser delayed 7 μs with respect to the ablating laser, crossing the plume 1 cm above the surface.

interacted with the plume perpendicularly to both the direction of the plume propagation and flight axis of the spectrometer. Ions produced by postionization were extracted by a pulsed field applied to the extracting/accelerating plates of the mass spectrometer by a high voltage switch (Behlke, GHTS 60) at controlled time delays with respect to the ablation and postionization laser pulses. In this way, positive ions formed directly by ablation are swept away from the extraction region and do not interfere with the detection of postionized species,[12] allowing time distribution measurements of neutral species. Also, the time distribution of SiO was obtained by LIF, exciting the $SiO(A^1\Pi v' = 3 \leftarrow X^1\Sigma v'' = 0)$ transition near 221.5 nm and collecting the $(A^1\Pi v' = 3 \rightarrow X^1\Sigma v'' = 8)$ fluorescence at 281−283 nm. For LIF measurements, vacuum conditions were also better than 2 × 10^{-6} mbar. The experimental setup has been reported in previous works.[18]

The structure of the cationic clusters observed in the ablation plume was investigated by density functional theory (DFT) calculations. The computations were performed by means of the suite of programs Gaussian03[20] with the theoretical model B3LYP/6-31G+(d). In all systems considered in this work, the calculated geometries were optimized at the same level, and energy minima structures were confirmed by frequency calculations.

3. Results and Discussion

3.1. Composition of the Plume. Mass spectra recorded at the ablation wavelength of 266 nm are shown in Figure 1a. Si_2O^+ is the most intense silicon oxide mass peak under a wide range of ablation conditions. Other Si-rich clusters, Si_3O^+, $Si_3O_2^+$, and weak features assigned to Si_4O^+ and $Si_4O_2^+$, are also observed, together with stoichiometric $(SiO)_n^+$ ($n = 1−4$). For $n = 1$ and 2, mass peaks assigned to $(SiO)_nH^+$ have higher intensities than the corresponding bare species; for $n = 3$ and

4, the mass features are better assigned to the bare clusters, although for $n = 4$, because of its weak intensity and partial overlap of the isotopic components, the presence of H-containing species cannot be fully excluded. Atomic silicon and Si_n^+ ($n = 2−10$) were also detected, although with very weak intensity for $n > 6$. The spectra also showed impurities with low ionization potentials Na^+, K^+, Li^+, and Al^+.

Some insight into the cluster formation mechanisms can be gained by comparing the plume composition obtained by 266 nm ablation with that reported by us in previous work.[11,12]

At 266 nm, Si_2O^+, Si_3O^+, and $Si_3O_2^+$ show the same relative intensities as those at 308, 540, and 532 nm, indicating that their formation process is quite insensitive to the laser target and laser plume interactions despite the differences in target absorption properties (nearly 1 order of magnitude larger at 308 nm than at 532 nm) and pulse duration (8 ns at 532 and 540 nm and 18 ns at 308 nm). This suggests that although ablation is carried out under vacuum, the small clusters observed in the present work can aggregate in the relatively dense region created near the target surface by barrierless or low barrier processes, similarly as predicted for small neutral clusters. For the latter, computational studies show that no barriers are present for $SiO + Si_2 \rightarrow Si_3O$ and $SiO + Si_2O \rightarrow Si_3O_2$ reactions.[21]

The relative intensity of stoichiometric $(SiO)_n^+$ clusters is higher at 266 nm than at longer wavelengths. As stated above, at 266 nm, $(SiO)_nH^+$ ($n = 1,2$) are stronger than the bare species; however, this cannot be discerned at longer ablation wavelengths because of broadening of the mass spectral features under the conditions at which they have appreciable intensity.

The intensity distribution of Si_n^+ clusters is significantly different at 266 nm than at longer ablation wavelengths. At 266 nm, the intensity of clusters with 6 to 11 atoms, recorded at different laser fluences and extraction conditions, is very weak. The opposite happens at 532, 540, and 308 nm; at these wavelengths, prominent $Si_6^+ - Si_{11}^+$ mass features are observed under a wide range of fluences,[11] with relative intensities that strongly resemble the intensity distribution of Si_n^+ products obtained in the dissociation of heavy Si_n^+ ($n > 30$) clusters.[22,23] This pattern can be accounted for only on the basis of the stability of products and therefore is largely independent of the dissociation source, either laser or collision-induced fragmentation.[23] The absence of the intense $Si_6^+ - Si_{11}^+$ characteristic fragmentation pattern indicates that effective formation of heavy Si_n^+ does not take place at 266 nm ablation. It should be noted that if $Si_6^+ - Si_{11}^+$ clusters were depleted by absorption within the ablation laser pulse duration, then it would result in Si^+ and Si_2^+ as the final products;[24] however, Si^+ and Si_2^+ signals are weak in the mass spectra of the plume at 266 nm ablation.

We suggest that the significant differences in Si_n^+ ($n = 6−11$) cluster intensity observed at long and short wavelengths could be related to the different effects induced on the target surface in each ablation region; at 308 nm and longer wavelengths, thermally induced disproportionation of the SiO target leads to the development of Si nanocrystals on the target, whereas at 266 nm and shorter wavelengths, there is evidence of the participation of an electronic ablation mechanism that does not yield Si nanocrystals, at least in the range of fluences used in this work.[17]

ArF laser postionization of the plume shows intense Si, SiO, and Si_2 mass peaks and much less intense Si_3 and Si_4. Similar plume composition was obtained at 308 nm ablation, although Si_n^+ clusters had relatively higher intensity and peaks up to $n = 7$ were observed at moderate fluences of ~0.6 J·cm^{-2}. At both wavelengths, SiO is the most intense species under different
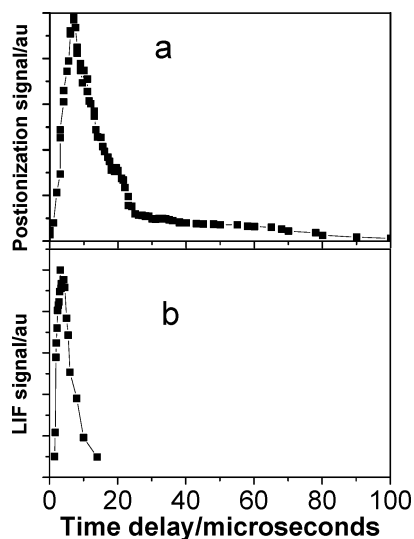
Figure 2. Time distributions of SiO at 266 nm. (a) Recorded by ArF laser postionization (fluence of 0.5 J·cm^{-2} and distance $l = 1.5$ cm). (b) Recorded by narrowband laser-induced fluorescence. ($F = 0.85$ J·cm^{-2}, $l = 1.5$ cm).

Figure 3. Calculated geometries of the most stable isomers of Si_2O^+, Si_3O^+, $Si_3O_2^+$, Si_4O^+, and $Si_4O_2^+$. The energies are relative to the most stable configuration (red oxygen atoms).

ablation fluences and time delays between postionization and ablation pulses. The mass spectrum is depicted in Figure 1b. Neutral silicon oxide clusters were not observed, similarly as reported at longer ablation wavelengths.[12] We note that within the $\Delta\lambda \approx 1$ nm bandwidth of the postionization, ArF laser heavier Si_nO_m clusters traveling in the plume at lower speed than SiO could be resonantly excited, some of which could undergo photofragmentation in the extraction region of the mass spectrometer, contributing to a delayed source of SiO.

The above possible channels can be discriminated by comparing the time distribution of SiO in the plume obtained by ArF laser postionization with the time distribution measured by selectively probing SiO by narrowband laser excitation ($\Delta\lambda$ narrower than 0.004 nm) of its rovibrational ($A^1\Pi v' = 3, N' \leftarrow X^1\Sigma v'' = 0', N''$) transitions near 221.5 nm. The results are presented in the next section.

3.2. Time Distribution of SiO in the Plume. The SiO time distribution measured by ArF laser postionization is depicted in Figure 2a. The distribution shows a complex shape with a maximum at ~ 7 μs and a shoulder at ~ 15 μs, followed by a long tail that lasts up to times longer than 100 μs. The relative contribution of this slow component increased with increasing fluence. Postionization signals of Si and Si_2 were also obtained at time delays longer than $60-80$ μs after ablation; these slow components could arise from heavy neutral Si_n clusters that would be formed in the ablation and then undergo extensive fragmentation within the ArF postionization laser pulse. However, the other source for Si and Si_2 formation is the dissociation of Si_nO_m clusters. In Section 3.3 below, a more detailed discussion on the fragmentation products of several Si_nO_m clusters will be given.

Figure 2b shows LIF of a single rovibrational transition of the ejected SiO selectively excited with a narrowband dye laser. The slow component of the time distribution is not observed, and the fast component reaches its maximum at shorter time than that of the time distribution obtained by postionization, indicating that in the latter, several sources contribute to the SiO mass signal.

Besides fragmentation of heavier Si_nO_m species, other possible source of the above delayed components could arise from ArF postionization of metastable excited states of SiO. The electronic
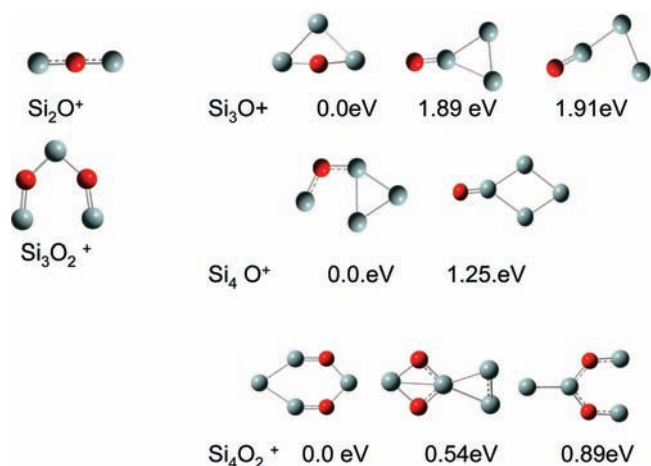
structure of SiO has been widely investigated by both theoretical and experimental methods. The lowest excited states are the triplet $a^3\Sigma^+$ and $b^3\Pi$ lying 4.14 and 4.21 eV, respectively, above the ground $X^1\Sigma^+$ state.[25,26] The spin forbidden transitions $a^3\Sigma^+ \rightarrow X^1\Sigma^+$ and $b^3\Pi \rightarrow X^1\Sigma^+$ have been observed experimentally,[27] and the emission lifetimes are calculated to be in the range of milliseconds,[26] although collisional quenching could considerably shorten the above lifetimes. However, detection of SiO ($^3\Sigma^+$ and $b^3\Pi$) by postionization requires the absorption of two ArF laser photons that, even from the lowest vibrational $v = 0$ state, would excite the molecule ~ 5.4 eV above the ionization threshold and thus ~ 0.42 eV over the ion dissociation limit into $Si^+(^3P_u)$ and $O(^3P)$.[26] Although this mechanism could contribute to the delayed Si signal observed in postionization, it would not account for the delayed Si_2 formation reported above.

Therefore, we tentatively conclude that the most plausible mechanisms contributing to the slow components of the SiO time distribution arise from resonant excitation, within the relatively wide bandwidth of the ArF postionization laser ($\Delta\lambda \approx 1$ nm), of neutral silicon oxide clusters formed in the ablation, followed by fragmentation into SiO; this would lead to different components of the SiO time distribution delayed with respect to the primarily formed SiO. For Si_nO_m clusters ($n = 12-18$), theoretical calculations indicate that the preferred dissociation pathway would produce a small pure silicon cluster or Si-rich oxide clusters plus a stable silicon oxide molecule.[2] Moreover, experimental work shows that the loss of one SiO unit is also the main fragmentation channel of stoichiometric $(SiO)_n^+$ clusters.[28]

In the next sections, aiming at getting some insight into the processes involved in the postionization of $Si_nO_m^+$, we have investigated the possible isomerization and dissociation channels by the study of the clusters most stable configurations and energies.

3.3. Structure of Nonstoichiometric $Si_nO_m^+$ Clusters Formed in the Ablation. Structure optimizations of positively charged nonstoichiometric Si_2O^+, Si_3O^+, $Si_3O_2^+$, Si_4O^+, and $Si_4O_2^+$ were performed, starting from a high number of possible candidate structures and taking into account the reported Si−O bonding distance.[6,14] The results are shown in Figure 3. Up to our knowledge, no previous calculations of $Si_nO_m^+$ clusters are available, except for Si_2O^+ and Si_3O^+. For the latter, ring geometries have been reported;[13] however, although for Si_2O^+, we also find a local minimum in the potential energy surface at

Silicon Oxide Cluster Formation and Stability

J. Phys. Chem. A, Vol. 113, No. 41, 2009 **10883**
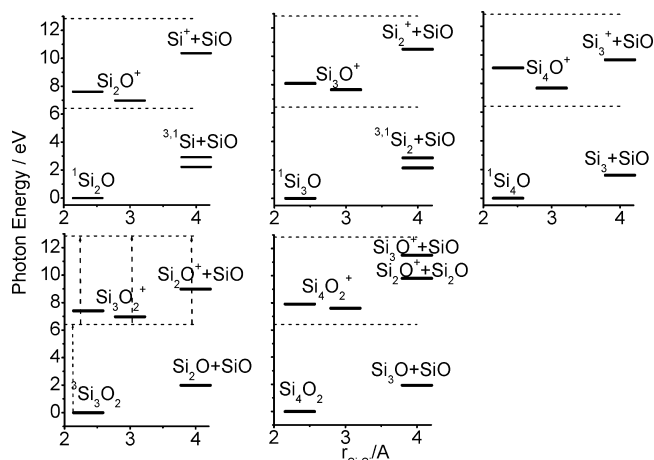
Figure 4. Energy level diagram of $Si_nO_m^{0/+}$ cluster states and lowest dissociation channels available by one- and two-photon ArF laser excitation (postionization). Vertical arrows indicate the different regions of the potential energy surface from which second-photon ionization could take place during the 14 ns ArF pulse duration.

TABLE 1: Calculated Ionization Energies of SiO and Si_nO_m

	SiO	Si_2O	Si_3O	Si_4O	Si_3O_2	Si_4O_2
VIP/eV	11.54^a	7.06	8.09	9.09	7.4	7.9
AIP/eV		6.98	7.65	7.68	6.97	7.6

^{a} Experimental value is 11.6 eV.

a Si−O−Si angle near 102°, the linear geometry shown in Figure 4 is 0.35 eV more stable. For Si_3O^+, the optimized geometry obtained in the present work is a nonplanar closed structure with the O atom out of the plane of the three Si atoms.

To obtain ionization energies and to estimate the energy available for Si_nO_m cluster fragmentation by photon absorption of the ArF postionization laser, we performed calculations of the respective neutral clusters and of SiO, Si_2, and Si_3 at the same level of theory. The most stable isomers obtained in the present work for Si_2O, Si_3O, and Si_4O are similar to previously reported calculations under different theoretical approaches.[14,21] For Si_3O_2 and Si_4O_2, triplet and singlet planar ring structures are, respectively, found in agreement with other results,[6,21] although different isomers are found to be more stable under other approaches.[14,21,29] The calculated vertical and adiabatic ionization energies are listed in Table 1. Our calculations are in good agreement with previously reported data for SiO, Si_2, Si_2O, and Si_3O.[13,29]

Regarding the differences observed between the structures of Si_nO_m neutral and cation clusters, natural bond orbital (NBO) population analysis shows that the excess of positive charge created by the removal of one electron is shared by the Si atoms straining the cluster structure; the cation energy stabilizes, breaking Si−Si or Si−O bonds or adopting elongated geometries.

The cluster ionization pathways and lowest spin-allowed fragmentation channels opened by ArF laser photon absorption of Si_nO_m are depicted in Figure 4. The energy diagram illustrates the possible mechanisms for SiO delayed formation. The lowest dissociation channel of neutral clusters gives SiO plus $Si_{n-1}O_{n-1}$ products; the calculated dissociation energies are in the range of 1.5 to 2.5 eV, which is in agreement with previously reported data.[14] The calculated ionization potentials are in the range of 7.0−9.5 eV, and the energy required to dissociate the most stable $Si_nO_m^+$ isomer into SiO plus $Si_{n-1}O_{n-1}^+$ is in the range of 2.0−4.0 eV. Therefore, absorption of one laser photon by excited states of the neutral clusters would place energy in

excess above their respective dissociation limits, whereas two-photon absorption is required for ionization. In clusters of moderate size, internal conversion of the states initially excited by one-photon absorption is on the order of picoseconds,[30] which is very fast in comparison with the nanosecond laser pulse; internal conversion into the ground state, followed by cluster dissociation, can compete with ionization by a second laser photon, then minimizing the ionization yield in favor of fragmentation processes. It has been shown in several works that reduced or null fragmentation can be achieved when postionization of neutral clusters is carried out by multiphoton ionizations with ultrafast femtosecond laser pulses[29] or by one-photon ionization with short-wavelength lasers.[31]

We tentatively conclude that neutral clusters in the plume, reaching the interaction region with the postionization laser at longer times than the primarily formed SiO, undergo fragmentation providing a route for delayed formation of SiO in the plume; this leads to the complex time distribution of SiO shown in Figure 3a and precludes the observation of neutral clusters by two-photon ionization with nanosecond ArF laser pulses.

3.4. Structure of Stoichiometric and H-Containing Clusters. The most stable structures of positively charged $Si_nO_n(H_{0,1})^+$ ($n = 1-4$) are shown in Figure 5. The structures of H-containing clusters were calculated starting from a large number of geometries and with the H atom facing either Si or O. For bare $Si_3O_3^+$ and $Si_4O_4^+$, several isomers were found very close in energy within a narrow interval of ∼0.5 eV; the calculated geometries were in agreement with those reported in recent work.[28] Clusters up to $n = 3$ have planar geometries with only Si−O bonds. Clusters with $n = 4$ were 3D rings with only Si−O bonds or structures containing one Si atom coordinated to three or to four O atoms in a tetrahedral geometry. Si−O bond distances were in the range of 1.5 to 1.9 Å.

No previous calculations have been reported for H-containing clusters. In the optimized $SiOH^+$ and $Si_2O_2H^+$ structures (observed in the mass spectra with more intensity than their corresponding bare cluster), the H atom is bonded to one O atom with bond distances smaller than 1 Å. For the most stable $Si_3O_3H^+$ and $Si_4O_4H^+$ isomers, H bonds to one Si atom; the Si−H bond distances are in the range of 1.1 to 1.5 Å. The exoergicity of the reactions $Si_nO_n^+ + H \rightarrow Si_nO_nH^+$ was also calculated, showing that the formation of hydrogenated clusters is energetically favorable in all cases.

The analysis of the NBO populations can provide some understanding of the structure of H−Si and H−O bonds. In Table 2, the natural populations calculated for several $Si_nO_n^+$ ($n = 1-4$) isomers and the respective clusters with H−Si and O−H bonds are listed. H−O formation involves electron population transfer from the H atom to the cluster, leaving a positive natural charge in H. When H bonds to a Si atom in the cluster, some small redistribution of the charge occurs in the system, leaving a higher positive NBO population on the Si atom involved in the bond and a small, close to zero, negative NBO charge in the H. The higher relative stability of Si−H containing clusters in $(SiO)_nH^+$ ($n = 3$ and 4) can be understood by the presence in these structures of low coordinated Si atoms with sp^2 and sp^3 hybridization, which are stabilized by the addition of hydrogen.

Hydrogen can be present at the surface of siliceous materials in the form of SiOH defects.[9] In many oxides, in contact with atmospheric water, hydroxyl groups are formed at the surface, and their density can play an important role in the absorption properties[32] and in a number of applications.[33] In metal oxides, hydrogen can be bound to O atoms or to the metal atom; for
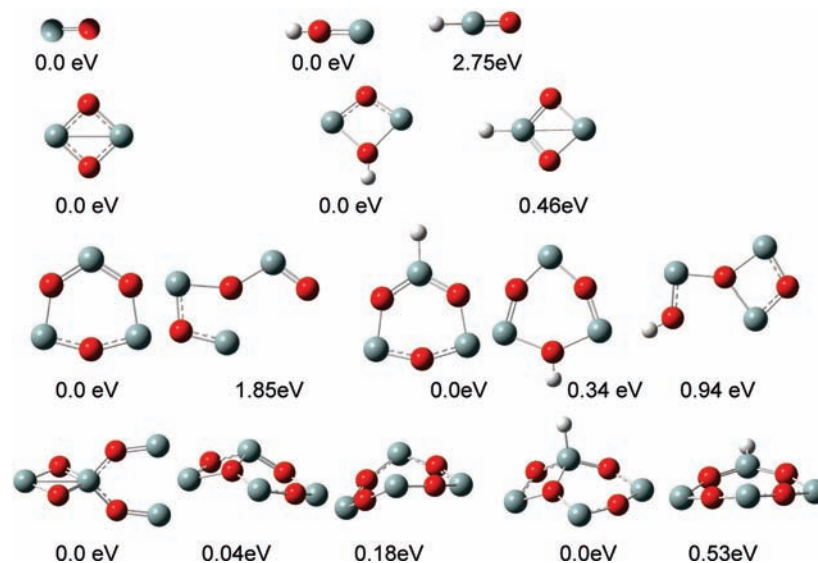
Figure 5. Calculated geometries of the most stable isomers of $(SiO)_nH_{0,1}^+$ ($n = 1-4$). Energies are relative to the most stable configuration of the respective bare or H-containing cluster.

TABLE 2: NBO Populations of $Si_nO_nH_{0,1}^{+a}$

	E/eV	Si*	Si	Si	Si	O*	O	O	O	H
0.0 eV		1.83				-0.83				
R-OH+	0.0	1.61				-1.23				0.62
R-SiH+	2.75	1.94				-0.9				-0.04
0.0 eV		1.72	1.72			-1.22	-1.22			
R-OH+	0.0	1.51	1.51			-1.25	-1.36			0.59
R-SiH+	0.46	2.06	1.5			-1.22	-1.22			-0.11
0.0 eV		1.93	1.55	1.55		-1.41	-1.32	-1.32		
R-OH+	0.34	1.51	1.48	1.48		-1.23	-1.41	-1.41		0.57
R-SiH+	0.0	2.14	1.51	1.51		-1.42	-1.29	-1.29		-0.14
0.04 eV		1.97	1.47	1.49	1.5	-1.41	-1.4	-1.28	-1.34	
R-SiH+	0.0	2.12	1.47	1.49	1.49	-1.41	-1.39	-1.27	-1.32	-0.18
0.18 eV		1.64	1.64	1.64	1.64	-1.39	-1.39	-1.39	-1.39	
R-OH+	1.14	1.47	1.49	1.49	1.47	-1.22	-1.42	-1.40	-1.42	0.56
R-SiH+	0.53	2.16	1.51	1.49	1.51	-1.33	-1.33	-1.43	-1.43	-0.16

[a] Si or O atom bound to H in the cluster.

instance, in TiO_2, no TiH species have been found in the surface, whereas in the less-reducible ZnO, both OH and ZnH species have been observed.[33] In silicon oxide materials, theoretical calculations on the equilibrium geometry of SiO_2 surfaces indicate that H bridges to oxygen atoms bonded to only one Si.[32]

A possible mechanism of formation of $Si_nO_nH^+$ could be started by desorption of hydrogen from the target surface during ablation, followed by reaction in the plume; however, the fact that hydrogenated nonstoichiometric clusters or $Si_3O_3H^+$ are not present in the mass spectra, despite the fact that its formation processes are exoergic, suggests that the observed $SiOH^+$ are not formed by reactions in the plume but directly ejected from the target surface at which only O−H defects would be present.

This mechanism would not generate species involving Si−H bonding, as in the most stable isomers of $Si_3O_3H^+$ and $Si_4O_4H^+$.

4. Conclusions

The generation of neutral and positively charged silicon oxide clusters in the laser ablation of SiO target at 266 nm has been investigated. Indirect evidence suggests that heavy neutral Si_nO_m clusters may be formed in the ablation, which undergo fragmentation within the nanosecond pulse of the postionization ArF laser and thus preclude their observation by this probing technique.

The bonding structure of $Si_nO_nH^+$ ($n = 1-4$) clusters was also investigated. The results show that only clusters with O−H

Silicon Oxide Cluster Formation and Stability

J. Phys. Chem. A, Vol. 113, No. 41, 2009 **10885**

bonds are formed in the ablation. It is tentatively concluded that H-containing clusters are directly ejected in the ablation from the target surface containing a large density of Si−O−H defects.

References and Notes

(1) Zhang, R. Q.; Zho, M. W.; Lee, S. T. *Phys. Rev. B* **2004**, *93*, 095503.

(2) Wang, H.; Sun, J.; Lu, W. C.; Li, Z. S.; Sun, C. C.; Wang, C. Z.; Ho, K. M. *J. Phys. Chem. C* **2008**, *112*, 7097.

(3) Zhang, R. Q.; Lifshits, Y.; Lee, S. T. *Adv. Mater.* **2003**, *15*, 635.

(4) Wang, N.; Zhang, Y. F.; Tang, Y. H.; Lee, C. S.; Lee, S. T. *Phys. Rev. B* **1998**, *58*, R16024.

(5) Morales, A. M.; Lieber, C. M. *Science* **1998**, *279*, 208.

(6) Chu, T. S.; Zhang, R. Q.; Cheung, H. F. *J. Phys. Chem. B* **2001**, *105*, 1705.

(7) Patrone, L.; Nelson, D.; Safarov, V. I.; Sentis, M.; Marine, W. *J. Appl. Phys.* **2000**, *87*, 3829.

(8) San Andrés, E.; del Prado, I.; Mártil, E.; González-Díaz, G.; Bravo, D.; López, F. J.; Fernández, M.; Bohne, W.; Röhrich, J.; Selle, B.; Sieber, I. *J. Appl. Phys.* **2003**, *94*, 7462.

(9) Schenkel, T.; Schlathölter, T.; Newman, M. W.; Machicoane, G. A.; McDonald, J. W.; Hamza, A. V. *J. Chem. Phys.* **2000**, *113*, 2419.

(10) Han, M.; Zhou, J. F.; Song, F. Q.; Yin, C. R.; Liu, M. D.; Wan, J. W.; Wang, G. H. *Eur. Phys. J. D* **2003**, *24*, 269.

(11) Torres, R.; Martin, M. *Appl. Surf. Sci.* **2002**, *193*, 149.

(12) Torres, R.; Jadraque, M.; Martin, M. *Appl. Phys. A: Mater. Sci. Process.* **2005**, *80*, 1671.

(13) Nayak, S. K.; Rao, B. K.; Khanna, S. N.; Jena, P. *J. Chem. Phys.* **1998**, *109*, 1245.

(14) Lu, W. C.; Wang, C. Z.; Nguyen, V.; Schmidt, M. W.; Gordon, M. S.; Ho, K. M. *J. Phys. Chem. A* **2003**, *107*, 6936.

(15) Lai-Sheng, W.; John B., N.; Michel, D.; Hongbin, W.; Steven D, C. *Phys. Rev. Lett.* **1997**, *78*, 4450.

(16) Zang, Q. J.; Su, Z. M.; Lu, W. C.; Wang, C. Z.; Ho, K. M. *Chem. Phys. Lett.* **2006**, *430*, 1.

(17) Díaz, L.; Santos, M.; Torresano, J. A.; Castillejo, M.; Jadraque, M.; Martín, M.; Oujja, M.; Rebollar, E. *Appl. Phys. A: Mater. Sci. Process.* **2006**, *85*, 33.

(18) Jadraque, M.; Martín, M.; Santos, M.; Díaz, L.; Sawczak, M.; Sliwinski, G. *J. Phys.: Conf. Ser.* **2007**, *59*, 293.

(19) Chelikowsky, J. R. *Phys. Rev. B* **1998**, *57*, 3333.

(20) Frisch, M. J.; Trucks, G. W.; Schlegel, H. B.; Scuseria, G. E.; Robb, M. A.; Cheeseman, J. R.; Montgomery, J. A., Jr.; Vreven, T.; Kudin, K. N.; Burant, J. C.; Millam, J. M.; Iyengar, S. S.; Tomasi, J.; Barone, V.; Mennucci, B.; Cossi, M.; Scalmani, G.; Rega, N.; Petersson, G. A.; Nakatsuji, H.; Hada, M.; Ehara, M.; Toyota, K.; Fukuda, R.; Hasegawa, J.; Ishida, M.; Nakajima, T.; Honda, Y.; Kitao, O.; Nakai, H.; Klene, M.; Li, X.; Knox, J. E.; Hratchian, H. P.; Cross, J. B.; Bakken, V.; Adamo, C.; Jaramillo, J.; Gomperts, R.; Stratmann, R. E.; Yazyev, O.; Austin, A. J.; Cammi, R.; Pomelli, C.; Ochterski, J. W.; Ayala, P. Y.; Morokuma, K.; Voth, G. A.; Salvador, P.; Dannenberg, J. J.; Zakrzewski, V. G.; Dapprich, S.; Daniels, A. D.; Strain, M. C.; Farkas, O.; Malick, D. K.; Rabuck, A. D.; Raghavachari, K.; Foresman, J. B.; Ortiz, J. V.; Cui, Q.; Baboul, A. G.; Clifford, S.; Cioslowski, J.; Stefanov, B. B.; Liu, G.; Liashenko, A.; Piskorz, P.; Komaromi, I.; Martin, R. L.; Fox, D. J.; Keith, T.; Al-Laham, M. A.; Peng, C. Y.; Nanayakkara, A.; Challacombe, M.; Gill, P. M. W.; Johnson, B.; Chen, W.; Wong, M. W.; Gonzalez, C.; Pople, J. A. Gaussian 03, revision B.05; Gaussian, Inc.: Wallingford, CT, 2004.

(21) Avramov, P. V.; Adamovic, I.; Ho, K.-M.; Wang, C. Z.; Lu, W. C.; Gordon, M. S. *J. Phys. Chem. A* **2005**, *109*, 6294.

(22) Zhang, Q.-L; Liu, Y.; Curl, R. F.; Tittel, F. K.; Smalley, R. E. *J. Chem. Phys.* **1988**, *88*, 1670.

(23) Jarrold, M; Honea, E. *J. Phys. Chem.* **1991**, *95*, 9181.

(24) Bloomfield, L. A.; Freeman, R. R.; Brown, W. L. *Phys. Rev. Lett.* **1985**, *54*, 2256.

(25) Field, R. W. *Phys. Scr.* **1976**, *14*, 298.

(26) Chattopadhyaya, S; Chattopadhyay, A.; Das, K. K. *J. Phys. Chem. A* **2003**, *107*, 148.

(27) Linton, G.; Capelle, G.A. *J. Mol. Spectrosc.* **1977**, *66*, 62.

(28) Garand, E.; Goebbert, D.; Santambrogio, G.; Janssens, P. L.; Meijer, G.; Neumark, D. M.; Asmis, K. R. *Phys. Chem. Chem. Phys.* **2008**, *10*, 1502.

(29) Reber, A. C.; Paranthaman, S.; Clayborne, P. A.; Khanna, S. N.; Castleman, A. W. *ACS Nano* **2008**, *2*, 1729.

(30) Foltin, M.; Stueber, J.; Bernstein, E. R. *J. Phys. Chem. A* **2001**, *114*, 8971.

(31) Matsuda, Y.; Shin, D. N.; Bernstein, E. R. *J. Chem. Phys.* **2004**, *120*, 4165.

(32) John, S. R.; Leraas, J. A.; Langford, S. C.; Dickinson, J. T. *Appl. Surf. Sci.* **2007**, *253*, 6283.

(33) Yin, X. L.; Calatayud, M.; Qiu, H.; Wang, Y.; Birkner, A.; Minot, C.; Wöll, Ch. *ChemPhysChem* **2008**, *9*, 253.